Intensified upwelling: normalized sea surface temperature trends expose climate change in coastal areas

Miguel Ángel Gutierrez-Guerra[1,2], María Dolores Pérez-Hernández[1], Pedro Vélez-Belchí[2]

[1] Unidad Océano y Clima, Instituto de Oceanografía y Cambio Global, IOCAG, Universidad de Las Palmas de Gran Canaria, ULPGC, Unidad Asociada ULPGC-CSIC, Canary Islands, Spain

[2] Centro Oceanográfico de Canarias, Instituto Español de Oceanografía, Santa Cruz de Tenerife, Canary Islands, Spain

Corresponding author: Miguel A. Gutierrez-Guerra, miguel.gutierrez104@alu.ulpgc.es

Abstract.

The Eastern Boundary Upwelling Systems (EBUS) provide valuable natural resources due to their high primary production. However, there is significant uncertainty in how climate change may affect the mechanisms that sustain these ecosystems in the future. Therefore, assessing the effects of climate change on the EBUS under the current global warming scenario is crucial for efficient ecosystem management. In 1990, Andrew Bakun suggested an increase in the upwelling intensity due to the rise of the ocean-land pressure gradient. Since there is a significant link between thermal gradients and offshore Ekman transport, we use sea level pressure (SLP) and deseasonalized sea surface temperature (SST) data from remote sensing to elucidate this hypothesis and validate it using in-situ observations. SST is an indicator of coastal upwelling, and our long-term analysis of monthly and deseasonalized SST records shows that the seasonal and synoptic processes have minimal influence on the SST-upwelling intensity relationship. Upwelling within the same EBUS is not usually evenly distributed along coastlines, leading to upwelling in specific areas, upwelling centers. We compare the SST trends in the main upwelling centers of the four EBUS with those in open ocean waters through a new index, α_{UI}, designed to characterize upwelling changes in the EBUS. An adimensional number allows us to normalize the trends independently of the upwelling system and compare all of them. Furthermore, we have complemented the SST index with sea level pressure gradient data. This new index (supported by SLP gradient trends) indicates intensification in all the EBUS, revealing a coherent pattern within EBUS in the same ocean (i.e., Canarian and Benguela or Californian and Humboldt Upwelling Systems).

1. Introduction

The world's major coastal upwelling areas exist along the eastern margins of the Pacific and the Atlantic Oceans. These extended coastal upwelling systems are known as Eastern Boundary Upwelling Systems (EBUS) and sustain the most important fisheries in the world (Pauly and Christensen, 1995). The rise of cool, nutrient-rich waters supports the high primary production needed to maintain these complex ecosystems (Ekman, 1905). Their economic and ecological relevance explains the association of the EBUS with the world's major Large Marine Ecosystems (LME) (Fig 1). LME are a globalized approach to a management framework that defines and ranks marine regions based on their gross primary production (Sherman and Hempel, 2008), and four of the largest LME are embedded in the EBUS worldwide (Kämpf and Chapman, 2016).

Bakun, (1990) hypothesized that the sea-land temperature gradient will increase under climate change and therefore, it should increase the upwelling intensity. The hypothesized increase in the temperature gradient arises from an increased atmospheric pressure gradient between the low-pressure cell that develops over the heated land mass and the high-pressure cell existing over the colder ocean. Therefore, as the land warms faster than the ocean, it enhances the low-pressure cells. Thus, the increase in the pressure gradient drives more intense upwelling favorable winds, intensifying the cold imprint in the Sea Surface Temperature (SST) near the shore. However, previous studies that have tested Bakun's hypothesis with in-situ data have found contradictory long-term trends (Barton et al., 2013; Belkin, 2009; McGregor et al., 2007; Rykaczewski et al., 2015; Sambe et al., 2016).

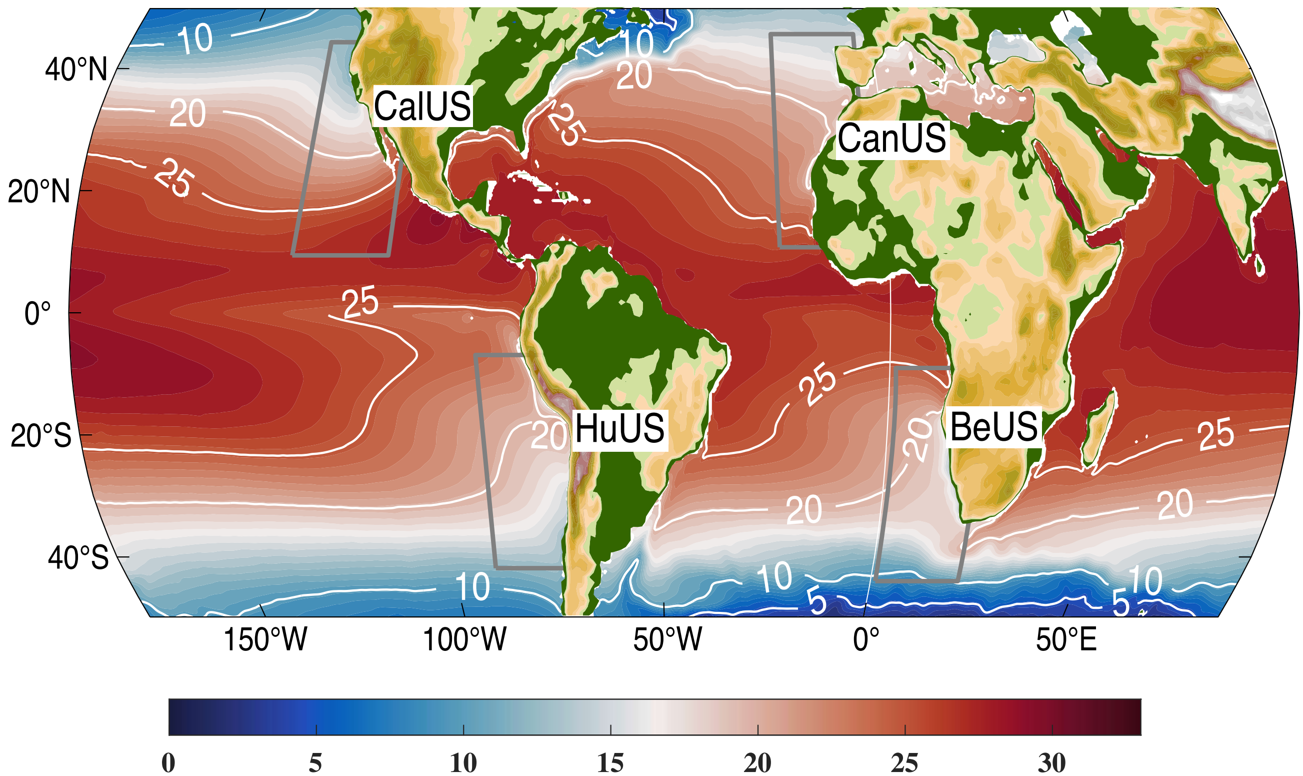

Fig 1: Location of the EBUS (enclosed and labelled areas) in the world, associated with eastern boundary currents.

Sydeman et al., (2014) performed a meta-analysis of 18 trends obtained from independent studies of wind stress, both from observational and model data. Observational data were more likely to report an increase in wind stress in the four EBUS than model data (excluding Benguela, where no observations were considered). However, the model data were less consistent between EBUS, showing agreement with observations only in the case of the California system (both supporting intensification) and for the Iberian system (with a consistent weakening of the wind stress). García-Reyes et al., (2015) also remarked that in climate change models, the upwelling-related cooling trends were difficult to reproduce due to the small spatial scale of the coastal upwelling process. Such a controversy between the model, and different observations reflects the complexity of EBUS dynamics.

Upwelling within the same EBUS is not usually evenly distributed due to irregular coastlines and seafloors, resulting in more pronounced upwelling in specific 'upwelling centers'. In these areas, the sea surface temperature (SST) drops significantly as cold subsurface water rises, leading to a stronger relationship between SST and upwelling intensity (Kämpf and Chapman, 2016). Consequently, these upwelling centers exhibit a stronger signal-to-noise ratio between SST and Ekman transport, making them ideal for studying long-term upwelling trends.

The main motivation of this study is to assess the impacts of climate change on the four EBUS. This is pursued by using satellite-derived SST trends as a proxy for changes and a new index that normalizes the upwelling trend of the coastal upwelling with the oceanic background trends. Specifically, we have chosen points representative of each dynamical regime at each EBUS: offshore oceanic waters (OC1), non-upwelling (DW1) areas nearshore, and upwelling centers (UP1 and UP2). These points were chosen based on the consistency of the year-round upwelling centers deduced from the mean SST field and the relevance of the area as spawning and nursery emplacements for the pelagic fisheries associated with upwelling centers. Then, we compare the SST trends in the main upwelling centers of the four EBUS with those in open ocean waters through a new index, α_{UI}, designed to characterize upwelling changes in the EBUS, following Bakun's (1990) hypothesis. The manuscript is organized as follows: sections 2 and 3 describe the dataset and the analysis carried out in the study. Section 4 describes the relevant results, which are discussed and contrasted with other studies, and finally, Section 5 summarizes and presents the conclusions.

2. Data

We based our study on the SST blended analyses for sea surface temperature of the National Ocean and Atmosphere Administration (NOAA) (Reynolds et al., 2007), which combines SST satellite retrievals with in-situ measures from ships and buoys. This dataset has a spatial resolution of 0.25º and covers nearly 40 years (from 1982 to 2021). Following Barton et al. (2013), the 40 years used in this study allow us to estimate significant trends. Their analysis involved a comprehensive examination of both wind stress and SST. They segmented these datasets into various subsets of different lengths. Within this analysis, the trends derived from wind datasets are not significantly different from zero for all considered subset periods.

In contrast, SST trends demonstrated statistical significance with a 40-year length dataset. In addition, we incorporated reliable in-situ data in the North Pacific and the North Atlantic oceans for validation. These records were obtained from the National Buoy Data Center (NDBC) and the CalCOFI (California Cooperative Fisheries Investigations) program for the Pacific. For the Atlantic, the data were gathered from Puertos del Estado and the RaProCan (Radial Profunda de Canarias) observational program of the Spanish Institute of Oceanography in the Canary Islands (Tel et al., 2016). The in-situ data, limited to the northern hemisphere, is used to validate the satellite observations. Given the significantly greater density existing in the Pacific Ocean compared to the Atlantic Ocean, a lower error is expected in the reanalysis for the Pacific Ocean. We have also used the EN4 (ENhanced ocean data assimilation and climate Prediction) dataset from the Met Office Hadley Centre (Good et al., 2013), a collection of global observations from diverse sources interpolated into a monthly product and a spatial resolution of 1º. Due to the limited sampling in the cruise data, we cannot align it with the monthly resolution of the EN4 product. To maintain statistical rigor, we choose not to employ the cruise data for the validation of EN4.

Additionally, two sea level pressure (SLP) datasets are used: the NCEP and ERA5 reanalysis data. The ERA5, from the European Centre for Medium-Range Weather Forecasts, offers a high resolution of ~0.25 degrees and uses advanced data assimilation methods, covering the period from 1950 to present. While the NCEP/NCAR Reanalysis, from the National Centers for Environmental Prediction and the National Center for Atmospheric Research, offers a resolution of 2.5 degrees and covers the period from 1948 to present.

3. Method

3.1. Selection of Representative Dynamical Regimes in EBUS.

We have selected areas representative of the different dynamical regimes for further analysis, to avoid mixing observations in dynamically different areas. Areas UP1 and UP2 are year-round upwelling centers. The DW1 are areas of convergence where the upwelling does not dominate on an annual average, and these areas are characterized by higher SST averages than those in the upwelling centers. The OC1 is representative of open ocean (>100 km offshore) areas with trends driven by Global Warming. Given the distinctive and unique features that characterized each EBUS, as commented in Section 1, we based the selection of the representative locations on the literature and the SST mean field (Fig. 2):

Californian Upwelling System (CaIUS)

In the Californian system, the strongest wind stress takes place in spring in the southern portion of the CalUS. In summer the strongest winds occur offshore of northern California around 38° N. This wind stress pattern diminishes as we move away from this latitude in both directions (Bakun and Nelson, 1991). Among the four regions depicted by Kämpf and Chapman (2016), the strongest upwelling occurs in two well-known upwelling centers (see Fig 2a) that we have selected for the analysis in this study: Cape Mendocino (UP1) (Abbott and Zion, 1987) and north to Point Conception (UP2) (Dugdale and Wilkerson, 1989), south of it, the wind's seasonal variability is different.

Canarian Upwelling System (CanUS)

Following Kämpf and Chapman (2016), the CanUS is divided into two distinct upwelling areas, which experience limited continuity of flows between them. This division arises due to the coastline interruption in the Strait of Gibraltar that leads to two upwelling areas: the Iberian Upwelling System and the Canarian Upwelling System. Given the lack of permanent upwelling centers in the Iberian Upwelling System, we have focused on the Canarian Upwelling System. Following Cropper et al. (2014), we selected the two upwelling centers (UP1 and UP2) on the cold SST cores (see Fig 2b) within the permanent upwelling area.

Humboldt Upwelling System (HuUS)

The HuUS is characterized by prominently strong upwelling zones along the Peruvian-Chilean coastline, due to the topographical influence of headlands, as described by Figueroa & Moffat, (2000) and Mesias et al., (2003). Notable regional upwelling centers encompass the continental shelf near Pisco (13.7°S), Antofagasta (21-25ºS), and the Mejillones Peninsula (23°S), as well as extending further south to

Coquimbo Bay (30°S), Valparaíso (33° S), and the Bay of Concepción (37°S). Moreover, in the Mejillones Peninsula (23°S), both observational (e.g., Marín, 2003) and modeling studies (Escribano et al., 2004) have revealed that the dynamics of coastal ecosystems in this area heavily rely on the generation of upwelling filaments. Additionally, the continental shelf near Pisco (13.7°S) emerges as an exceptionally productive and distinctive upwelling center. Hence, the two upwelling centers (Fig 2c) selected are Pisco (UP1) and the Mejillones Peninsula (UP2).

Benguela Upwelling System (BeUS)

As Kämpf and Chapman (2016) described, within the Benguela Upwelling System, numerous upwelling centers extend along the shelf area of the Benguela Current region. These centers include Cape Frio (18.5°S), Walvis Bay (22.95°S), Lüderitz (26.45°S), Namaqualand (28.55°S), Cape Columbine (32.85°S), and Cape Town (33.95°S). Lüderitz stands out as a particularly noteworthy upwelling center within this system (Andrews and Hutchings, 1980; Lutjeharms and Meeuwis, 1987; Peard, 2007). As Hutchings et al. (2009) defined, Lüderitz represents an intensive perennial upwelling center characterized by intense winds, high turbulence, and robust offshore transport. Another significant area of interest lies in Cape Columbine, primarily due to its biological importance (Andrews and Hutchings, 1980; Bang and Andrews, 1974; Andrews and Cram, 1969). Given these distinctive features, we have selected Lüderitz (UP1) and Cape Columbine (UP2) as the upwelling centers for our analysis (Fig 2d).

3.2. Trends Analysis

With a minimum data length of over 30 years, a climate series can usually be described as a combination of multiple variabilities at different time scales. Since we are interested in the trend of the record, we removed the high-frequency variability (<1 yr) by averaging the daily NOAA SST analyses data (1982-2021) into monthly means and removing the seasonal cycle. The seasonal cycle is a recursive signal throughout the entire record, and therefore, it does not influence the trend but induces noise in the target scale. The monthly climatology was subtracted from the record to remove the seasonal cycle. After this pre-analysis, we calculated the trend with the ordinary least square method. We evaluated the strength of these correlations using the Pearson Correlation Coefficient (PCC). The following qualitative classification will be used throughout the manuscript: Perfect (1), very high (>0.9), high (>0.7), and moderate (>0.5). Additionally, we employed the simple Mann-Kendall (MK) test to evaluate the statistical robustness (Kendall, 1975; Mann, 1945). The MK tests verify whether an n-length series holds a monotonic increase or decrease trend. In addition, we need to consider the instrumental error since, historically, a warm coastal bias is found in satellite records compared to in-situ records (Smale and Wernberg, 2009). This bias was assessed in the northern hemisphere by validating the data using in-situ observations. Additionally, to assess the drivers of change in upwelling intensity, we calculated the sea level pressure gradients for each EBUS. The gradients were calculated between the cores of the high- and low-pressure systems (exact positions provided in supplementary material, Fig S1). To corroborate more recent hypothesis that suggests an alternative mechanism, a poleward shift of the oceanic high-pressure system would stimulate latitude-dependent changes in the magnitude and timing of the upwelling winds (Rykaczewski et al., 2015). A displacement of the pressure systems would increase the standard deviation of the trends around their cores.

3.3. Angular Index of Upwelling Intensification (α_{UI})

To test Bakun's hypothesis, a new index, named the Angular Index of Upwelling Intensification (α_{UI}), is proposed. This new index uses the angle between the trend of the most robust upwelling cell at each EBUS and the trend at the corresponding open ocean area. If the upwelling intensifies, as Bakun proposed, the trends in the open ocean and the cell are expected to differ significantly, resulting in a higher angle between the trends. To calculate α_{UI}, two vectors (in the time-temperature space) may be constructed from the upwelling ($\overrightarrow{Up}$) and oceanic ($\overrightarrow{Oc}$) trends. The rotation sense (clockwise or anticlockwise) is used to calculate the relative orientation of ($\overrightarrow{Up}$) over ($\overrightarrow{Oc}$), needing to consider an additional unit vector ($\vec{n}$) normal to $\overrightarrow{Up}$ and $\overrightarrow{Oc}$

The mathematical formulation of α_{UI} is

$$\alpha_{UI} = arctan^{*}\left(\frac{\left(\left(\overrightarrow{Up}\ x\ \overrightarrow{Oc}\right)\cdot\bar{n}\right)}{\overrightarrow{Up}\cdot\overrightarrow{Oc}}\right) = arctan\left(\frac{\left|\overrightarrow{Up}\right|\left|\overrightarrow{Oc}\right|\ sin(\alpha_{UI})}{\left|\overrightarrow{Up}\right|\left|\overrightarrow{Oc}\right| cos(\alpha_{UI})}|\bar{n}|\cos(\beta)\right)$$

* We used the four-quadrants arc tangent in this analysis since it allows to determine the sign of the angle based on the signs of the arguments.

Following the right-hand rule, if the cross product of $(\overrightarrow{Up})$ and $(\overrightarrow{Oc})$ is anticlockwise (that is, if the open ocean trend $(\overrightarrow{Oc})$ is greater than the upwelling trend $(\overrightarrow{Up})$, the resulting vector of the cross product has the same orientation as $\overline{n}$. This implies that the dot product $(\overrightarrow{Up}$x $(\overrightarrow{Oc})\cdot\vec{n}$ is positive since the angle (β) between $\vec{n}$ and $(\overrightarrow{Up}$ x $\overrightarrow{Oc})$ is 0º. In case the upwelling trend is greater than the open ocean trend, $\overrightarrow{Up}$ x $\overrightarrow{Oc}$ results negative since β is now 180º. Note that this methodology is susceptible to the order of the vectors, as $\overrightarrow{Up}$ x $\overrightarrow{Oc}$=-$\overrightarrow{Up}$ x $\overrightarrow{Oc}$. Since we are interested in the relative position of the upwelling trend concerning the oceanic waters, the order used is $\overrightarrow{Up}$ x $\overrightarrow{Oc}$. It is important to note that the angle derived from trigonometric functions are not influence by units associated with the original vectors. Therefore, this new index is independent of temperature and time units.

We also conducted a probabilistic assessment of uncertainties for α_{UI}, taking into account the uncertainties associated with upwelling and open ocean SST series. We performed an error estimation using the Monte Carlo method: individual data points were separately and randomly sampled 10,000 times within their respective uncertainty ranges for (Up) and (Oc). These new sampled series were then used to calculate α_{UI}. The standard deviation of the 10,000 simulations represents the uncertainty of α_{UI}.

3.4. Satellite Validation

Taking advantage of the in-situ observations available in the study areas defined in Fig 2, we performed a validation through linear regression between in-situ and the deseasonalized satellite data. Records with no systematic error correspond to a linear regression slope with a value of 1 (perfect). Since the Pacific Ocean is better sampled than the Atlantic, better reanalysis performance and higher correlation are expected in the Pacific Ocean.

4. Results

4.1. Satellite Validation

We first carried out a regional validation, in the northern hemisphere, with in-situ observations (Fig 2a and 2b) to test the consistency of the NOAA SST analyses between oceans. A linear fit between in-situ and satellite data gives insights into the reliability of the SST data in both oceans. As described in Section 2, the in-situ dataset was divided into two categories: mooring and cruise data. Because each record has a different spatial and temporal resolution, categories are not comparable. Nonetheless, all the linear fits are statistically significant.

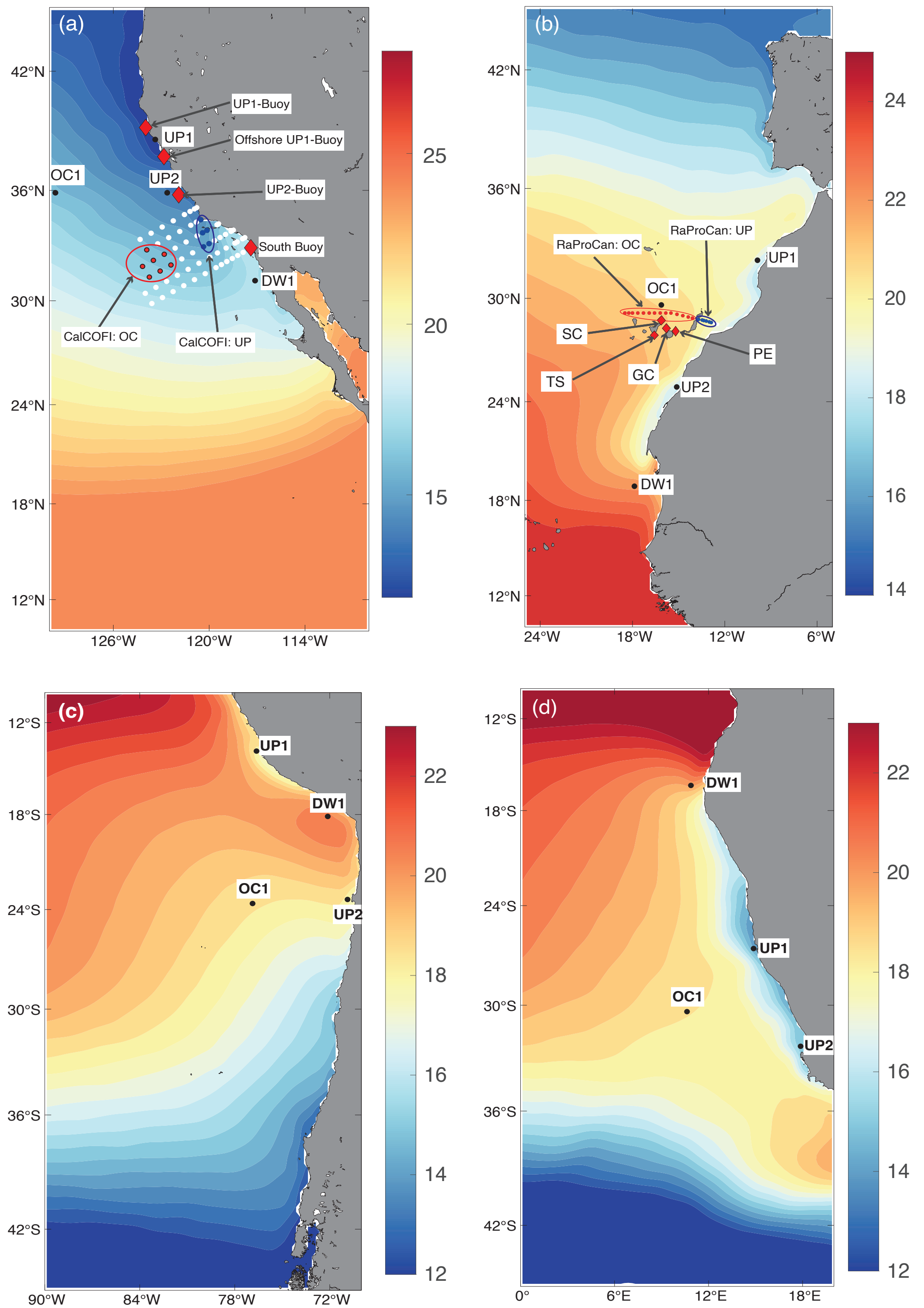
(a)
42°N
36°N
30°N
24°N
18°N
12°N
126°W
120°W
114°W
UP1-Buoy
UP1
Offshore UP1-Buoy
OC1
UP2
UP2-Buoy
South Buoy
DW1
CalCOFI: OC
CalCOFI: UP
25
20
15
(b)
42°N
36°N
30°N
24°N
18°N
12°N
24°W
18°W
12°W
6°W
RaProCan: UP
RaProCan: OC
UP1
OC1
SC
PE
TS
GC
UP2
DW1
24
22
20
18
16
14
(c)
12°S
18°S
24°S
30°S
36°S
42°S
90°W
84°W
78°W
72°W
UP1
DW1
OC1
UP2
22
20
18
16
14
12
(d)
12°S
18°S
24°S
30°S
36°S
42°S
0°
6°E
12°E
18°E
DW1
UP1
OC1
UP2
22
20
18
16
14
12

Fig 2: Average SST (ºC) maps for each of the Upwelling Systems: CalUS (a), CanUS (b), HuUS (c), and BeUS (d). Overlaid are the locations of the moorings (red diamond) and cruise data (black dots) used for the satellite validation with their corresponding names. The cruise stations were divided into upwelling (blue dots) and open ocean areas (red dots). The representative points of UP, DW, and OC in each basin are shown as black dots. The colour scales are presented at the right margin of each graph.

In the Pacific Ocean, the moorings selected were those as close as possible to the areas UP1, UP2, DW1, and OC1 described in section 3.1 and 3.4. We found the highest correlations inside the upwelling center of this region, where the UP1-Buoy and UP2-Buoy presented a linear regression fit of 0.99, supported by a very high correlation strength (0.94 and 0.92, respectively, Table 1). In the area where the upwelling meets the oceanographic background, the correlation of the offshore UP1-Buoy with the NOAA SST data decays slightly, presenting a linear slope of 0.84 and a correlation strength of 0.86. For the South-Buoy, close to DW1, the lineal fit and correlation (0.97 and 0.92) are closer to the values inside of the upwelling cell than of the offshore UP1-Buoy (Table 1). The results obtained for the offshore UP1-Buoy exemplify the effect of using a large averaging area surrounding the upwelling centers instead of a point, as the average introduces noise by adding points where upwelling might not be taking place, reducing the correlation in the transitional zone.

The cruise observations in the Pacific Ocean (CalCOFI) were divided into two different areas, open ocean (CalCOFI: OC) and upwelling (CalCOFI: UP), and we avoid data at transitional areas, as seen in Fig 2a. The results of the linear fit between the cruise and the reanalysis data are similar to those obtained with the mooring data (Table 1 and supplementary material Fig S2). The average within the upwelling cell, CalCOFI: UP, has a very high linear regression value (0.91), while for the offshore stations, CalCOFI: OC, the regression is 0.81. Nevertheless, the strength of the correlation is sensitive to the amount of data available from the cruise data in the ocean versus the upwelling areas. Additionally, due to the time resolution of the cruise, the correlation strength is moderate (0.68) for the CalCOFI: OC and high (0.71) for the CalCOFI: UP.

We also compared the EN4 dataset (Table 1, two last columns) against the NOAA SST analysis. As described in section 2, due to the coarse temporal resolution of the cruise data, it was not possible to compare with the EN4 monthly. Overall, the EN4 has lower correlation and regression values than the NOAA SST analyses. The correlation has the same pattern in both datasets (NOAA and EN4): moderate in the northern locations (0.60 and 0.63) and high in the southern locations (both with 0.76), although the data length of the EN4, unlike the cruise records, is the same as the mooring.

	NOAA		**EN4**	
In-situ Data	Linear Slope	Correlation	Linear Slope	Correlation
UP1-Buoy (46014).	0.99	0.92	0.70	0.60
Offshore UP1-Buoy (46028).	0.84	0.86	0.72	0.63
UP2-Buoy (46225).	0.99	0.94	0.78	0.76
South-Buoy (46026).	0.97	0.92	0.77	0.76
CalCOFI: OC	0.81	0.71	-	-
CalCOFI: UP	0.91	0.68	-	-

Table 1. Values of the linear regression and Pearson's correlation strength between the in-situ data (listed in the first column, with the designation within the manuscript and, in brackets, the official NDBC station ID). The in-situ data are compared with the NOAA SST reanalysis (second and third columns) and the EN4 product (last two columns) validation for the Pacific Ocean. The last two rows are for the CALCOFI cruise data of the Pacific Ocean.

In the Atlantic Ocean, the number of in-situ measurements available is more limited than in the Pacific Ocean. Therefore, the long-term records are shorter than in the Pacific Ocean and are only available in the surroundings of the Canary Islands. The results reflect these limitations since none of the linear regressions or correlation coefficients ever exceeds 0.9, unlike the results for the Pacific Ocean (Table 1). As in the Pacific Ocean, the mooring data shows a better linear regression and higher correlation coefficient than the cruise data (Table 2 and supplementary material, Fig S3). The correlation coefficients for the buoys of Santa Cruz, Gran Canaria, and Tenerife Sur are high, with values of 0.89 (0.84), 0.84 (0.87), and 0.83 (0.88), respectively. The result of Las Palmas East-Buoy is comparable to the linear slope for the cruise data, 0.71. However, the Las Palmas East-Buoy has a higher correlation coefficient (0.89), which agrees with the other moorings.

For the cruise data, we follow the same approach as in the Pacific Ocean, dividing the data into open ocean areas (RaProCan: OC) and upwelling centers (RaProCan: UP). As occurred for the results in the Pacific, the regression is better for the upwelling cell with values of 0.73 and a correlation strength of 0.71. For the open ocean areas (RaProCan: OC), the linear slope is slightly lower (0.63) but has a higher correlation strength coefficient (0.77).

The EN4 dataset was also used in these areas and showed linear regressions and correlation coefficients similar to the cruise data, as shown in Table 1. In Table 2, the linear regressions of EN4 are close to the results of the moorings, even though EN4 performs similarly compared to Table 1. Thus, EN4 seems a better alternative in the Atlantic Ocean than in the Pacific Ocean, but only due to the lower performance of the NOAA SST analyses in the Atlantic Ocean. However, the correlation strength of the EN4 showed lower values than NOAA SST analyses, with three out of five locations under 0.70. Hence, using the NOAA SST analyses for long-term analysis in both oceans is a better approach.

	NOAA		**EN4**	
In-situ Data	Linear slope	Correlation	Linear Slope	Correlation
Las Palmas East Buoy.	0.71	0.89	0.80	0.71
Santa Cruz Buoy.	0.89	0.84	0.71	0.66
Gran Canaria Buoy.	0.84	0.87	0.76	0.54
Tenerife South Buoy.	0.83	0.88	0.77	0.53
RaProCan: OC	0.63	0.77	-	-
RaProCan: UP	0.73	0.71	-	-

Table 2. Values of the linear fit and correlation strength between in-situ data (listed in the first column) and both the NOAA SST analyses (second and third columns) and the EN4 product (last two columns) for the Atlantic Ocean. The last two rows are for the RaProCan cruise data of the Atlantic Ocean.

4.2. Trend patterns on the EBUS

We begin by identifying the overall pattern of the long-term trends in each EBUS, which we show in Fig 3. A general pattern of cooling (negative) trends within the upwelling centers and warming (positive) trends offshore is found in most of the regions. An exception is found in the HuUS, where there is also a cooling trend offshore. This cooling mode, however, is not as pronounced as the trends onshore driven by the upwelling process. On top of these general patterns, each region presents unique features that will be described in the following paragraphs.

The mean trend for the CalUS (Fig 3a) is 0.10 (SD= 0.06) ºC/decade. The minimum values, -0.17 ºC/decade, are located near Cape Mendocino, around 43-39ºN, and 32ºN corresponding to the permanent upwelling centers. On the other hand, maximum values (excluding the shallower Gulf of California), reaching up to 0.20 ºC/decade, are located south, at 30ºN, where the winds are non-favorable for year-round upwelling, and there is convergence (Kämpf & Chapman, 2016). At around 22 ºN, there is an offshore negative trend area with mean values of -0.02 ºC/decade. However, the MK test revealed that these trends in the offshore area are not significant. The extensive non-significant regions in the MK test support the idea that the trends in the CalUS coastal upwelling are only statistically distinguishable from zero within the upwelling centers.

In the CanUS (Fig 3b), the mean trend in the region is warmer than in CalUS, with a value of 0.20 (SD= 0.04) °C/decade. The minimum values (-0.20 ºC/decade) are confined to two upwelling centers in the permanent annual upwelling zones, located north of Cape Ghir and south of Cape Bojador. The maximum warming trend is 0.60°C/decade, located west of Cape Timiris in the Mauritania-Senegalese convergence zone. Because of the low spatial variability of the trend in the CanUS, the mean offshore value is the same as the average value of the entire CanUS.

For the HuUS (Fig 3c), the mean value of the region is 0.007 (SD= 0.09) ºC/decade. A cooling signal stands out as the general pattern in the tropic, with a mean value of -0.15 ºC/decade. Despite this cooling of the overall trend, there are two clear upwelling centers, at 13ºN and 24ºN, with minimum values of -0.36 ºC/decade. In these upwelling centers, the negative trends are stronger than in the open ocean at the same latitudes.

Finally, in the BeUS (Fig 3d), the mean trend is 0.19 (SD= 0.09) ºC/decade, closer to the average of the CanUS. Two warm fronts with trends over 0.40 ºC/decade can be found in the north and south ends. In the year-round upwelling area, the Lüderitz cell (Andrews and Hutchings, 1980; Lutjeharms and Meeuwis, 1987; Peard, 2007), the minimum value is -0.25 ºC/decade. In contrast, for the open ocean area between the two warm fronts, the values are similar to those found in the CanUS (Fig 3b), around 0.20 ºC/decade.

The average trend for each region reveals stronger open ocean warmings for the Atlantic EBUS (0.20 and 0.19 ºC/decade for the CanUS and BeUS, respectively) than the Pacific Ocean (0.10 and 0.007 ºC/decade, for the CalUS and HuUS, respectively), with the weaker trends observed in the HuUS. However, the trends along the coast are rather heterogeneous, responding to the variability of the local upwelling dynamics, as seen in Fig 3, where several permanent upwelling centers (negative trends) exist along the coast on both continents.

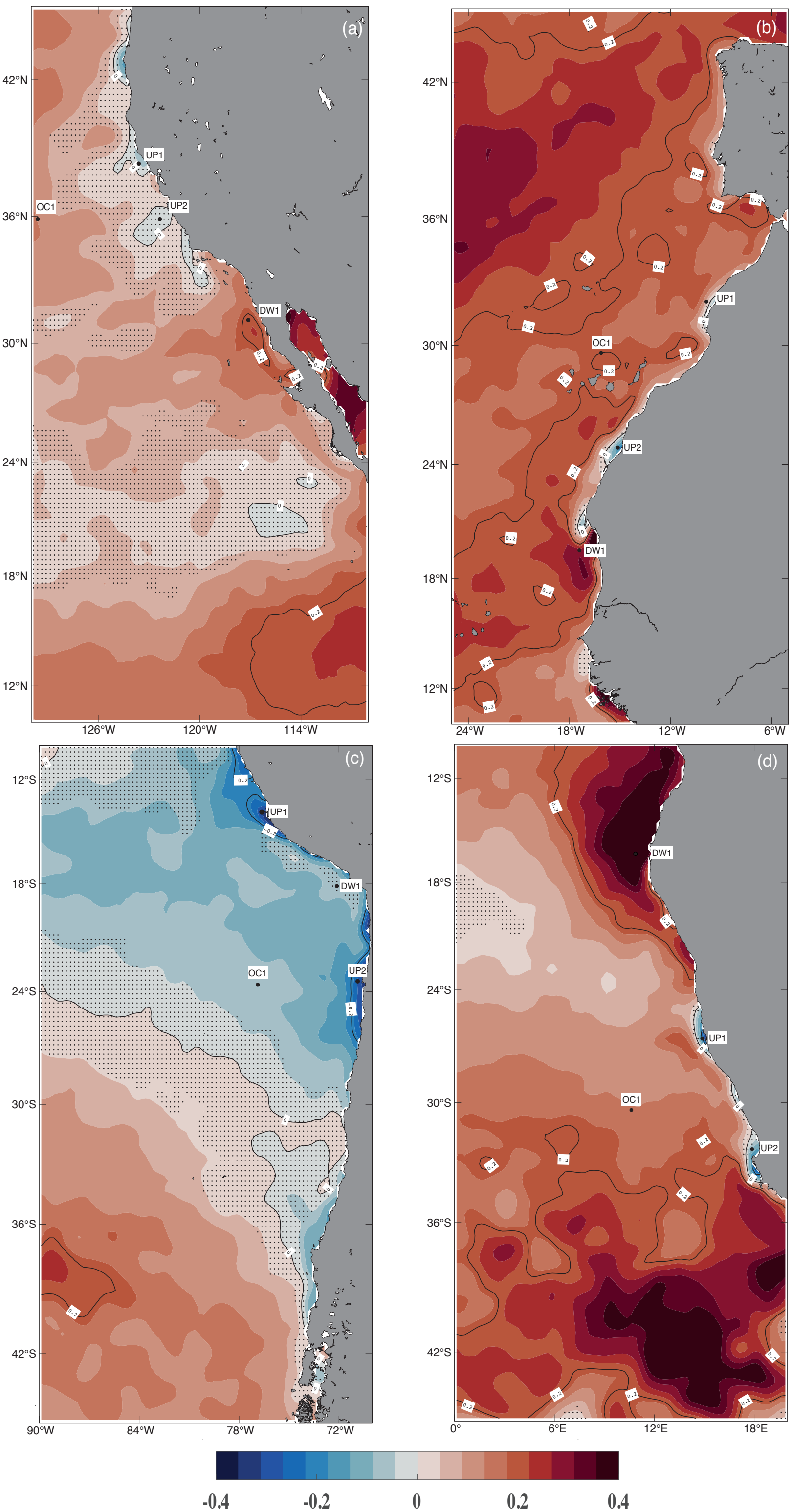
(a)
(b)
(c)
(d)
UP1
UP2
DW1
OC1
42°N
36°N
30°N
24°N
18°N
12°N
126°W
120°W
114°W
24°W
18°W
12°W
6°W
12°S
18°S
24°S
30°S
36°S
42°S
90°W
84°W
78°W
72°W
0°
6°E
12°E
18°E
-0.4
-0.2
0
0.2
0.4

Fig 3: Mapped SST trends (ºC/decade) for the major EBUS: a) California -CalUS, b) Canary-CanUS, c) Humboldt-HuUS, and d) Benguela-BeUS. The colour scale indicates the trend values at the bottom of the figure. Black-dots shaded areas indicate non-significant trends. The locations of the areas selected (UP1, UP2, OC1, and DW1) are marked with solid black circles and labelled with their names. Black contours enclosed the isotrends -0.20, 0, and 0.20°C/decade.

4.3. Trends in the upwelling cells and open ocean areas.

Although we got an overview of the long-term trends for each EBUS in the previous section, the validation of Bakun's hypothesis would require a finer resolution to describe the local dynamics of the upwelling and identify those areas where the coastal upwelling is the main forcing. In this sense, we have chosen representative points (see criteria in Section 3.4 and Figs 2 and 3) of both EBUS and non-EBUS areas instead of using the large-averaged regions shown in Fig 3. These points include the upwelling centers (UP1, UP2), the nearshore areas where the upwelling is not the primary process (DW1), and the open ocean areas (OC1).

The CalUS presents the weakest trends of all the EBUS in both year-round upwelling centers, being -0.06 ºC/decade for UP1 and non-significant in UP2 (-0.03 ºC/decade, Fig 4a). For the open ocean area, the OC1 trend is positive with a value of 0.14 ºC/decade, a lower value than the trend of 0.22º C/decade of the DW1. In the Atlantic, the CanUS (Fig 4b) possesses the only positive trend (0.07 ºC/decade) of all the EBUS in an upwelling area (UP1). Despite UP1 being positive, the trend is closer to zero than in the OC1 (0.20 ºC/decade). Furthermore, the UP2 cell in the CanUS shows a trend twice as negative (-0.15 ºC/decade) as the one in the CalUS upwelling UP1. The OC1 and DW1 areas show a warmer trend in the CanUS than in the North Pacific region (Fig 4). All of the above suggests that in the Northern Hemisphere EBUS, Bakun's hypothesis is fulfilled, and this is even more significant in the CanUS despite having been dismissed in previous studies (Sydeman et al., 2014).

In the HuUS (Fig 4c), we find a different behavior than the one seen in the other EBUS, showing negative trends in all the representative locations. The upwelling centers of the HuUS present the greatest cooling trend of all the EBUS, -0.30 ºC/decade at UP1 and -0.26 ºC/decade at UP2. As observed in CanUS, the values for HuUS in OC1 (0.06 ºC/decade) are similar to the ones of DW1, although DW1 is non-significant in the HuUS. Its counterpart in the Atlantic Ocean, the BeUS (Fig 3d), presents significant large negative trends in the year-round upwelling areas (-0.23 ºC/decade for UP1 and -0.10 ºC/decade for the UP2) and positive trends in OC1, 0.14 ºC/decade. The trend of the DW1 is the warmest (0.57 ºC/decade) found in all the EBUS, and it is related to the warm inflow from the Indian Ocean.

Overall, the trends show warming in the OC1 areas while cooling in the upwelling areas, except for the HuUS, where the trend at the OC1 is also slightly negative. The contrast between the trends of upwelling and open ocean areas found throughout the EBUS indicates upwelling intensification. To quantify this intensification, it is necessary to have an index that compares the intensification of the upwelling with the global warming trend in the open ocean area, that can be compared for all the EBUS. To compare the intensification between upwellings and to further understand the impact of the oceanic background on these trends, we will use the index α_{UI} described before to normalize the trends of each EBUS.

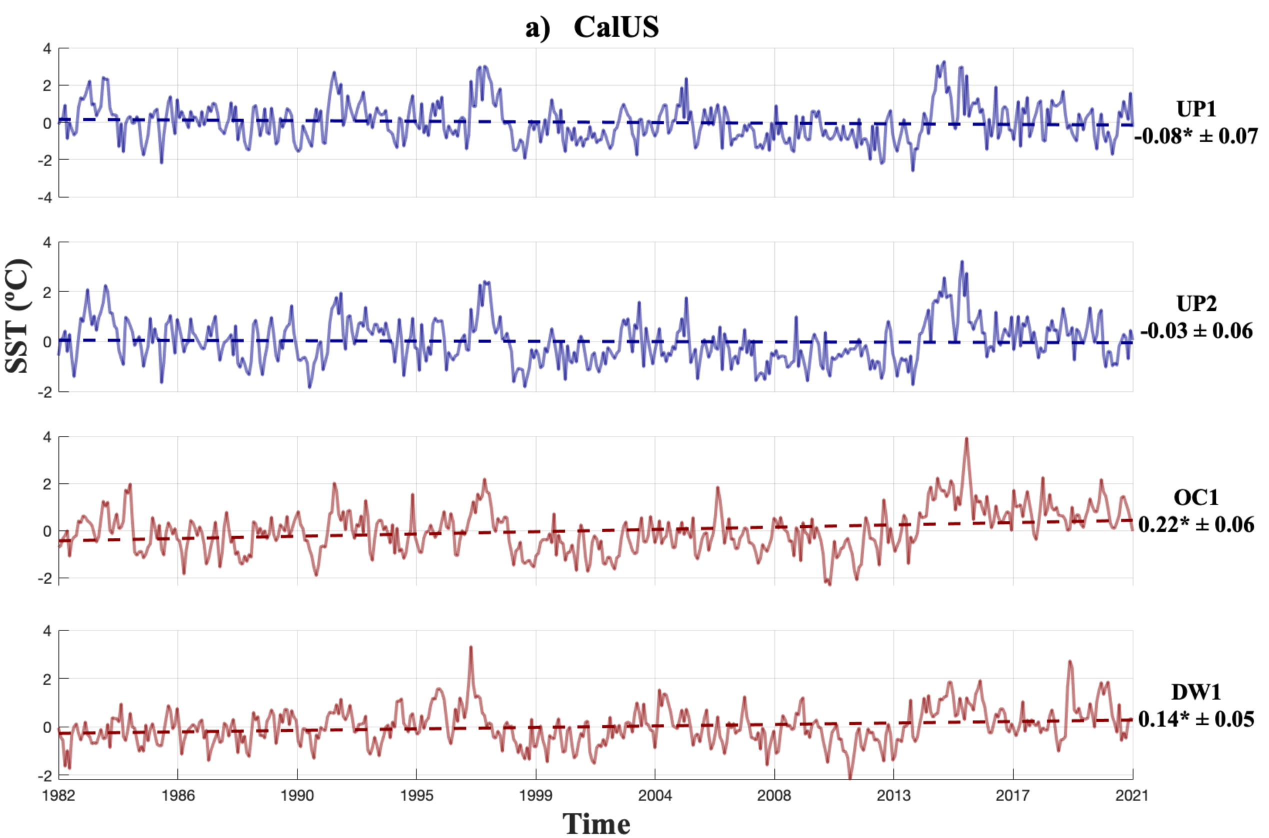

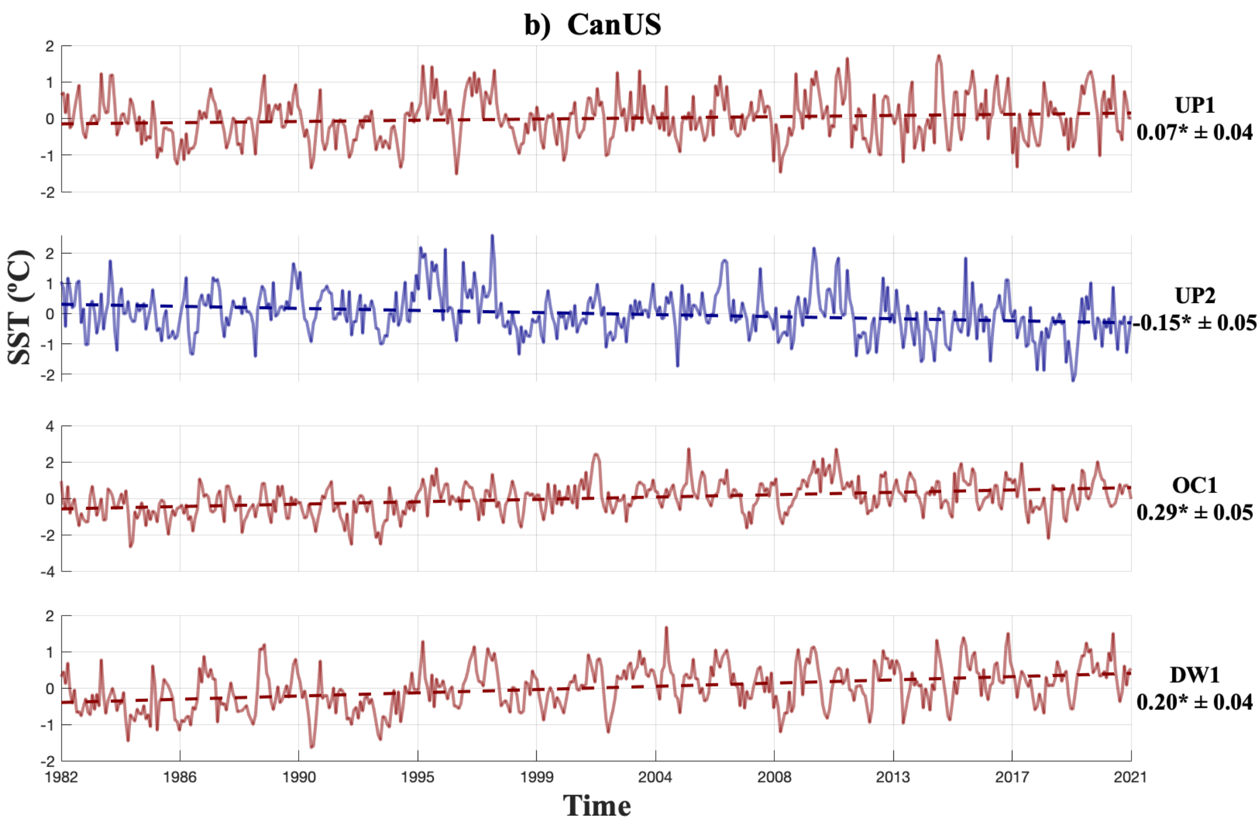
b) CanUS
SST (ºC)
UP1
0.07* ± 0.04
UP2
-0.15* ± 0.05
OC1
0.29* ± 0.05
DW1
0.20* ± 0.04
1982
1986
1990
1995
1999
2004
2008
2013
2017
2021
Time

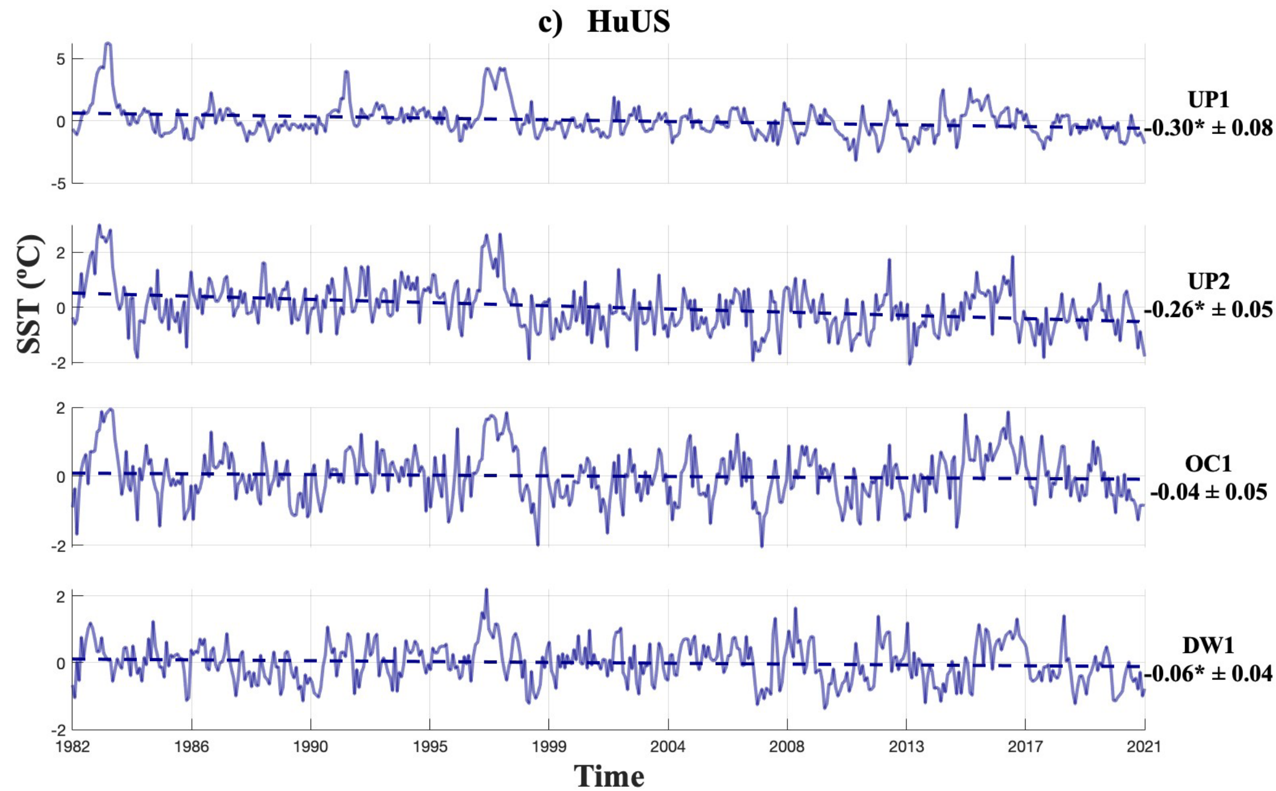
c) HuUS
SST (ºC)
UP1
-0.30* ± 0.08
UP2
-0.26* ± 0.05
OC1
-0.04 ± 0.05
DW1
-0.06* ± 0.04
Time
1982
1986
1990
1995
1999
2004
2008
2013
2017
2021

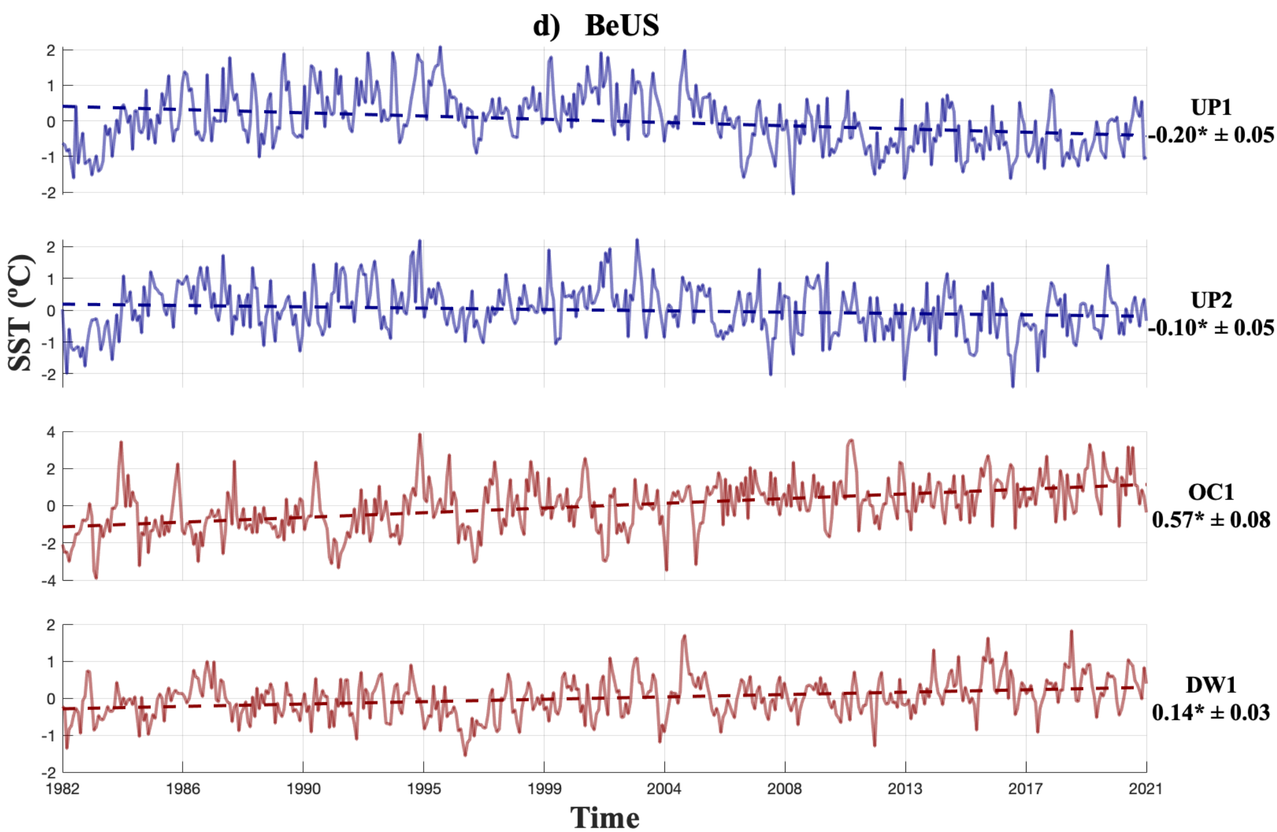

Fig 4: SST time series and trends (ºC/decade) for the selected areas for each one of the EBUS (DW1, UP1, and UP2) and the areas representative of the open ocean (OC1) in each EBUS: a) California, b) Canary, c) Humboldt and d) Benguela. The blue lines are for negative (cooling) trends, and the red ones are for positive (warming) trends. On the right side of the Y-axis, the trends are shown in ºC/decade, along with the area's label and confidence interval. Mann-Kendall significant trends (p-value<0.05) are marked with an asterisk next to their value.

4.4. The relation between Oceanic and EBUS trends.

Global warming induces the increase of oceanic SST, and under Bakun's hypothesis, it also enhances the favorable upwelling winds responsible for intensifying the upwelling areas. We define an angle between the upwelling and oceanic trends, as described in the methodology section, to discern Bakun's hypothesis from the global increase in SST. As described previously (Fig 4), the upwelling centers UP1 (except for the CanUS, where UP2 will be used due to the warming detected on UP1 in Section 4.3) have the strongest cooling, and we will use these trends (hereafter, in this section UP) to create the angle contrasts with the positive warming trend of the open ocean (OC1) area for each EBUS (Fig 4).

For CanUS, the α_{UI} obtained between the UP and OC1 trends is $20^{\circ} \pm 2^{\circ}$ whereas it is $11^{\circ} \pm 3^{\circ}$ in the CalUS, $21^{\circ} \pm 2^{\circ}$ for the BeUS, and $14^{\circ} \pm 3^{\circ}$ for the HuUS. The smallest angle is found in the CalUS because of the low cooling and warming trends described in Section 4.3. This result for the CalUS is coherent with the overall non-significant trends in the Mann-Kendall test (Fig 3a). The BeUS and CanUS have the highest contrast between the two regression lines (recall that we observed similar UP and OC1 trends in the Atlantic Ocean in Section 4.3) presenting similar α_{UI}.

The BeUS and CanUS show a weaker negative trend than the HuUS, but the oceanic background at the HuUS leads to a smaller angle. At the HuUS, a negative SST trend is observed for the whole study area. The existing hypotheses suggest that this trend is led either by a stronger cool phase of El Niño Southern Oscillation (ENSO) or related to the Southern Ocean SST changes (Meehl et al., 2016, Kang et al., 2023b, a). Nevertheless, at the HuUS, we have the most prominent upwelling negative trend. However, when normalized with the open ocean trend, the Bakun's effect is reduced. In the annual upwelling series of CalUS and HuUS, two prominent peaks associated with the warm phase of ENSO around 1983 and 1997. In general, we found positive α_{UI} for all the EBUS, supporting the intensification of the upwelling-oceanic gradient, as expected from Bakun's hypothesis.

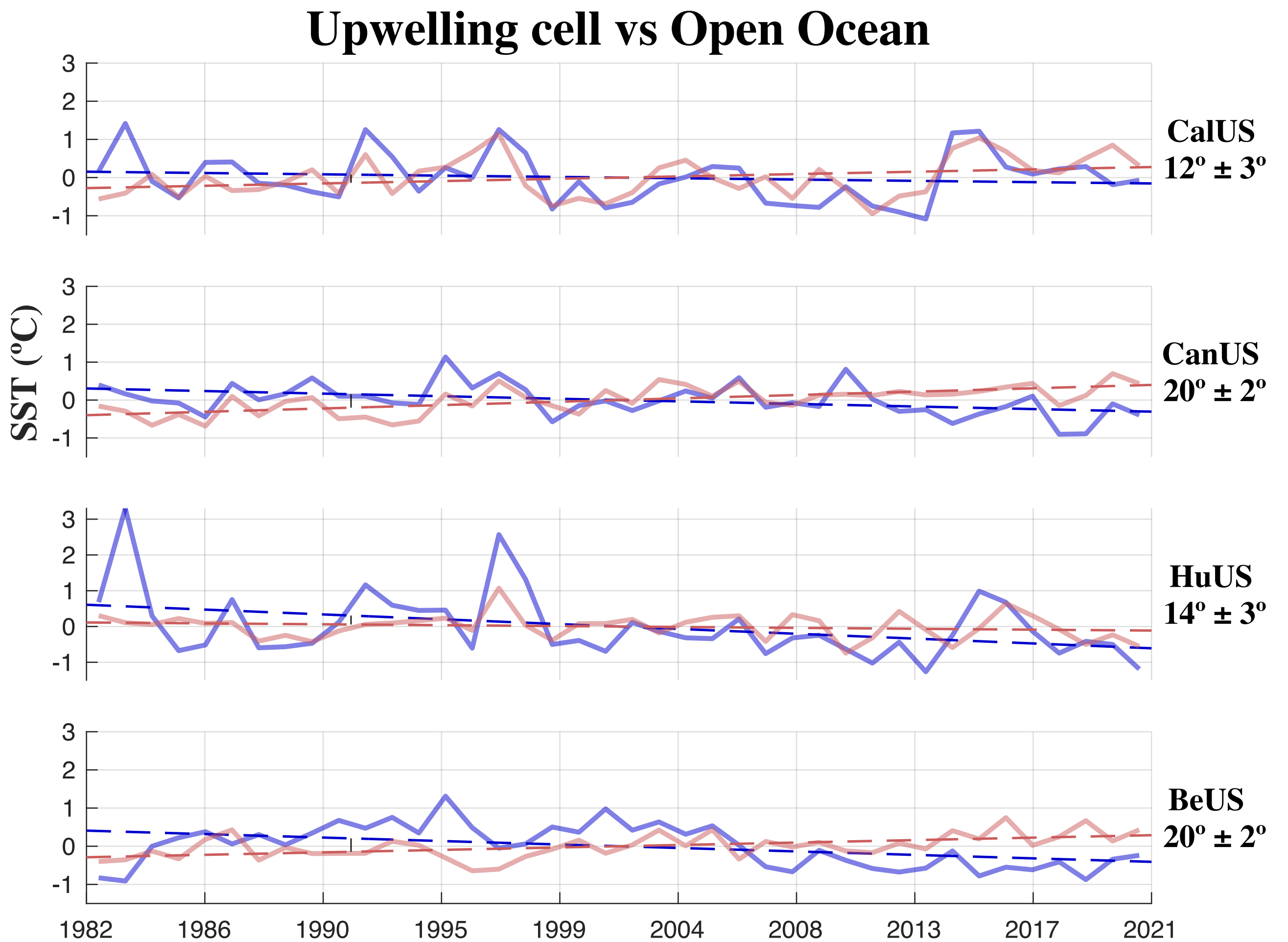

Fig. 5: EBUS SST trends (ºC/decade) against non-EBUS areas trends for each region. The EBUS annual series (continuous line) and trend (dotted line) are shown in blue; the same is true for the non-EBUS but is represented in red. On the opposite side of the Y-axis is labelled the α_{UI} with their corresponding EBUS.

4.5. Latitudinal distribution of α_{UI}

Many authors have previously tested the Bakun hypothesis, providing little consensus on both historical and projected records (Barton et al., 2013; Belkin, 2009; McGregor et al., 2007; Sambe et al., 2016, and Sydeman et al, 2014;). Such controversy has yielded alternative hypotheses to explain changes observed in the magnitude and timing of upwelling processes. Rykaczewski et al. (2015), suggests an alternative mechanism to the intensification of the upwelling process. They suggest a poleward shift of the oceanic high-pressure system which would stimulate latitude-dependent changes in the upwelling winds. To address this, we have calculated the latitudinal distribution of the α_{UI} (see Fig 6) in each EBUS. The spatial variability of the upwelling intensity proxy, α_{UI}, reveals distinct patterns and regional differences. In the CalUS, upwelling intensification demonstrates consistent upwelling activity between 35°N to 45°N with α_{UI} values reaching up to approximately 10° (Fig 6a). Conversely, in the CanUS, significant upwelling intensification is observed between 20°N and 30°N, with α_{UI} values peaking at 20º and in locations consistent with our dynamical analysis based on literature review (Fig 2b, UP1 and UP2). Similarly, in the HuUS upwelling intensification is confined to low latitudes (10-20 ºS, Fig 6c), and the values are close to those of the CalUS, (index values around 10º), as seen in the previous section. In contrast with the other regions, the BeUS shows intensification at high latitudes with maximum values of α_{UI} (20º) in the upwelling center of this region – Lüderitz upwelling center at 25ºS and Cape Columbine (around 32ºS)-. While results of BenUS and CalUS appear consistent with the findings by Rykaczewski et al, (2015), there is no supportive evidence in the other regions. To elucidate the possible mechanism responsible for such differences we will attend to the driver of the upwelling-favourable wind, the sea level pressure gradient

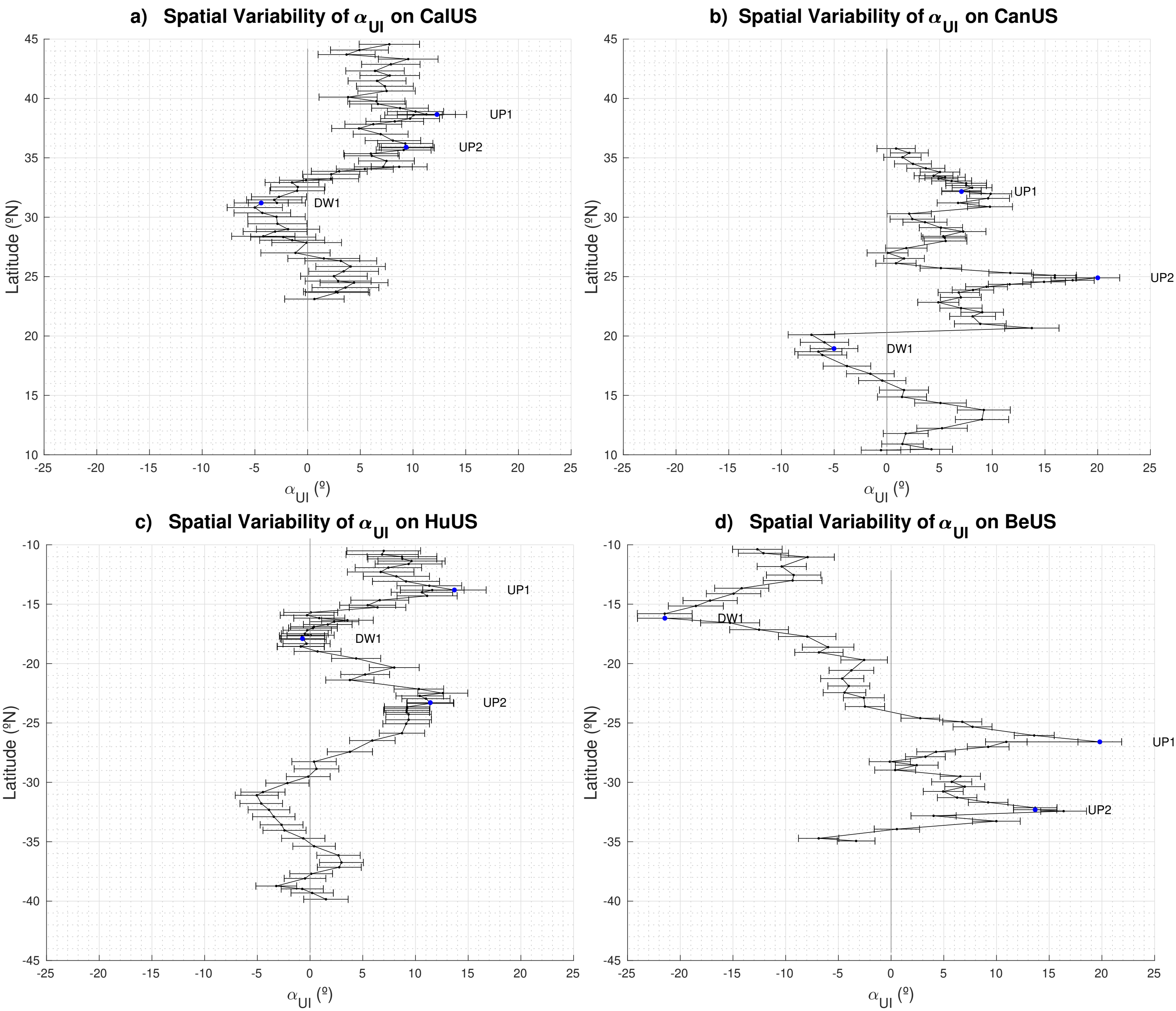

Fig 6: Spatial distribution of the α_{UI} (over the period of 1982-2021) along the coast for CalUS (a), CanUS (b), HuUS(c) and BeUS(c). The α_{UI} is calculated between grid points along the coast and OC1.

4.6. SLP Gradients

The coastal upwelling intensification postulated by Bakun mechanism, in 1990, would involve a stronger increase of near-surface temperature over land than over the ocean, which would lead to an intensification of the continental thermal low-pressure system relative to the ocean. To test this driver mechanism, we have calculated the trends (Fig 7) of the gradient between the continental thermal low and the oceanic high pressure.

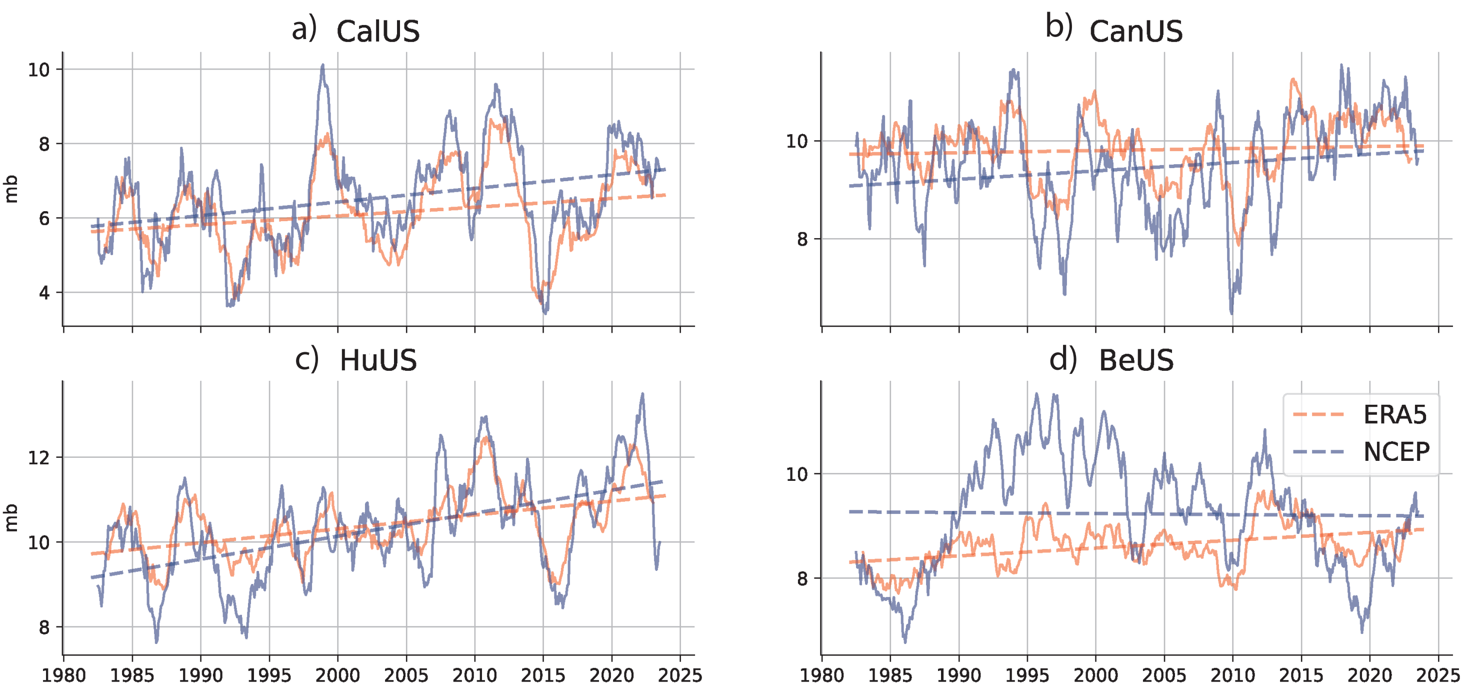

Fig 7: EBUS SLP gradients trends and temporal series for NCEP (blue lines) and ERA5 (red lines) datasets over the period 1982- 2023.

ERA5 data show positive and significant trends across all EBUS (see Table 3), while NCEP data indicate negative trends in the BeUS. Despite these differences, both datasets show good overall agreement. The strongest SLP gradient trends are found in the HuUS region, whereas the weakest trends occur in the BeUS. Given its coarser resolution (2º) compared to ERA5 (0.25º), NCEP data are considered less reliable. Despite these findings, both datasets support an intensification of the pressure gradient.

	CalUS (mbar/decade)	CanUS (mbar/decade)	HuUS (mbar/decade)	BeUS (mbar/decade)
ERA5	0.24 (0.039)	0.04 (0.017)	0.33 (0.038)	0.015 (0.051)
NCEP	0.37 (0.073)	0.17 (0.034)	0.54 (0.070)	-0.02 (0.072)

Table 3. Values of the trend, over the period 1982-2023, for the ERA5 (first row) and NCEP (second row) for all the EBUS. Parentheses enclose spatial standard deviation.

5 Discussion and Conclusions.

Bakun proposes an intensification of the upwelling due to the increase of the continental low-pressure system driven by global warming. However, controversies arise from discrepancies between wind stress datasets and differences in the methodologies used.

On one hand, Barton et al. (2013) highlighted a lack of consensus among various wind datasets, since they did not observe statistically significant changes in the meridional (upwelling-favorable) wind. These discrepancies in wind data are consistent with those noted by Narayan et al. (2010), who, despite finding significant increases in coastal upwelling areas when using COADS wind stress, also found that the NCEP/NCAR wind stress indicated a significant decrease in the upwelling off NW Africa, and a non-statistically significant trend for Lüderitz, California, and the Peruvian upwelling areas. Furthermore, they also observed that the ERA-40 dataset showed an increasing coastal upwelling in the NW African and Peruvian upwelling areas but a decrease in the California upwelling areas, with a non-statistically significant trend in the Lüderitz upwelling areas Therefore, using wind data as a proxy for upwelling leads to a wide spread of results as it strongly depends on the data product used.

On the other hand, SST-based indexes are usually constructed from thermal differences between coastal and offshore SST areas taken at the same latitude and following the coastline (Benazzouz et al., 2014; Gómez-Gesteira et al., 2008; Santos et al., 2012). This methodology does not consider the regional upwelling dynamics, and averages upwelling centers with areas without upwelling. Abrahams et al. (2021) introduced an upwelling metric based on marine heatwave detection techniques, examining favorable upwelling winds and SST data together. Their findings revealed a strong association between a decrease in SST and an increase in upwelling intensity. Their novel methodology holds significant importance in unraveling the connection between the physical upwelling phenomenon and its ecological impacts. However, predicting ecological impacts remains challenging. While intensified upwelling could mitigate habitat warming, it may also increase ocean acidification, hypoxic events and reduce suitable food for fish larvae (Abrahams et al., 2021; Bakun et al., 2015). Nonetheless, they successfully establish a link between decreased SST and changes in upwelling intensity, even when trends in wind dynamics do not fully account for the upwelling response, reinforcing the notion that SST is a suitable proxy for upwelling intensity. However, their SST metrics exhibited inconsistencies across upwelling areas, except for the Humboldt system. These inconsistencies may be due to the averaging of data across extensive areas, mixing upwelling areas with areas without the associated cold water of upwelling. Abrahams et al. (2021) also explored these metrics in upwelling-favorable winds data, and their results indicated that decadal trends were generally not significant. As previously discussed, wind products often yield contradictory results despite their direct relevance to upwelling. Hence, our study complements Abrahams et al. (2021) since we have focused on SST to understand longer terms changes in the upwelling intensity, using areas with optimal signal-to-noise ratio, namely the upwelling centers, revealing upwelling-related cool water in all Eastern Boundary Upwelling Systems (EBUS).

Therefore, in this study, we assess the intensification of the upwelling from a regional perspective, by using SST trends at locations representative of upwelling and of an open oceanic reference location for each different EBUS.

Additionally, we tested the effects of averaging areas on the index (see supplementary material, Fig S4 and Table S1). Our findings indicate that the averaged response is influenced by the dynamical regions involved, rather than by the size of the region averaged. This is evidenced by the invariant results when including the three coastal areas (DW1, UP1 and UP2). In contrast, focusing on specific upwelling zones, particularly around upwelling centers, made the intensification more evident. Moreover, we verified the stability of the trend both spatially and temporally by performing the analysis of Barton et al. (2013) across all the EBUS (supplementary material, Fig S5).

Furthermore, to assess the strength of the net upwelling intensification, we proposed an index that allows inter-basin comparisons attending to their regional background. SST, often used as an indicator of coastal upwelling, can be influenced by various factors, such as changes in surface mixing and offshore storm activity. However, in our long-term analysis of monthly and deseasonalized SST records, the seasonal and synoptic processes have minimal influence on the SST-upwelling intensity relationship. Moreover, Wang et al. (2015) explored the connection between sea-land thermal gradients and offshore Ekman transport using the CMIP5 models. Their findings underscore the significant link between thermal gradients and offshore Ekman transport, even under greenhouse gas emission scenarios. McGregor et al. (2007) and Santos et al. (2012) also support this relationship, emphasizing significant correlations between coastal SST and offshore Ekman transport, reinforcing the utility of coastal SST as a proxy for assessing upwelling intensity.

To assess the quality of our results, we validated the NOAA SST reanalysis with in-situ data from both the Atlantic and Pacific Oceans before estimating the trends in all EBUS. Overall, the Atlantic Ocean had lower correlations with the satellite data than the Pacific Ocean, likely due to shorter in-situ records. Nevertheless, we found high and robust correlation coefficients (>0.7) that sustain the satellite SST trends in oceanic and upwelling areas. We observed negative SST trends in all the EBUS, being stronger in the southern hemisphere (the strongest located in the HuUS-UP1 showing a trend of -0.30ºC/decade) than in the northern hemisphere (the weakest in the CalUS-UP2 with a trend of -0.06ºC/decade). Our results are consistent with the meta-analysis by Sydeman et al. (2014), who concluded, from observational and model data, that a significant intensification of upwelling exists, except for the case of CanUS.

Other studies have investigated the SST trends in the EBUS but with an approach that did not consider the heterogeneity of the upwelling areas. For instance, in the CalUS, Seabra et al. (2019) reported a 0.06ºC/decade warming rate, over the period 1982–2018. However, their approach involved averaging a 500 km nearshore area, excluding non-significant regions. Thus, almost half of the extension was not considered, resulting in the average of different dynamical areas and the exclusion of upwelling centers. Belkin et al. (2009) performed a similar analysis but included the entire CalUS nearshore area. They found a net change of -0.035 ºC/decade over the 1982-2007 period, agreeing in sign with our study but showing a weaker trend due to the use of a large average. In contrast, Siemer et al. (2021) found negative trends of -0.14ºC/decade, over the period 1982-2019, for the CanUS permanent upwelling area, like our results (-0.15ºC/decade). However, this trend fades away and becomes positive when they average the whole coastal upwelling area, highlighting the relevance of the methodology used in this study. Likewise, many studies carried out in this area present positive trends for the upwelling due to the method used (Belkin, 2009; Demarcq, 2009; Seabra et al., 2019). In line with our study, Seabra et al. (2019) found the largest cooling trends (-0.07 ± 0.08°C/decade) in the HuUS. However, like in other EBUS, using averaged areas increased the trend values. This pattern is also observed by Belkin et al. (2009), where the net change of the averaged nearshore area results in -0.05ºC/decade. For the BeUS, similar to CanUS, averaging the entire coastal upwelling area results in the fading of the observed upwelling trend. Hence, a warming rate of 0.17 ºC/decade is found in Seabra et al. (2019). In contrast, Santos et al. (2012) investigated trends, over the period 1982-2010, close to the shore without averaging areas and found a negative trend of the BeUS, strongly agreeing with our results (-0.13 ºC/decade). Hence, a warming rate of 0.17 ºC/decade is found in Seabra et al. (2019). In contrast, Santos et al. (2012) investigated trends close to the shore without averaging areas and found a negative trend of the BeUS, strongly agreeing with our results (-0.13 ºC/decade).

While all the upwelling trends are negative and support the Bakun's hypothesis, the oceanic trends behave differently across basins. We observed warming in all the open ocean areas except in the HuUS, where a cooling of –0.06ºC/decade is observed. Dong & Zhou (2014) studied the influence of the Interdecadal Pacific Oscillation (IPO) on Global Warming trends. Their EOF analysis results indicate that the transition to the negative phase of the IPO modes is responsible for the cooling trends observed in the Pacific.

The warming in the CalUS and BeUS is 0.14ºC/decade (over the period 1982-2023), while this trend is slightly more prominent in the CanUS. Seabra et al. (2019) revealed oceanic warming rates (0.06ºC/decade), over the period 1982–2018, on the averaged upwelling in CalUS lower than the OC1 trend (0.14ºC/decade). The open ocean positive trend of the CanUS is identical to the one in Siemer et al. (2021) and further agrees with other studies (Belkin, 2009; Good et al., 2007; Signorini et al., 2015). The result of Seabra et al. (2019) in HuUS also showed a very similar trend (-0.07 ºC) compared with our OC1 trend. Finally, in the BeUS, a good agreement is found with the average warming rate of Seabra et al. (2019). Our study demonstrates good agreement with existing literature on oceanic trends despite the differences in methodologies employed.

Although long-term changes, such as the North Atlantic Oscillation or the Pacific Oscillation, can impact the SST gradient, their effect would not surpass the ability of our analysis to support Bakun's hypothesis. In that sense, Nayaran et al. (2010) found that correlations between upwelling indices and climate indices like the Atlantic Multidecadal Oscillation Index (AMOI) lack significance. Similarly, the North Atlantic Oscillation Index (NAOI) exhibits a notable negative correlation with meridional wind stress off NW Africa, yet its correlation with the SST index remains insignificant. In the case of the CalUS, the Pacific Decadal Oscillation Index (PDOI) shows a weak but statistically significant correlation with the coastal upwelling SST index off California. However, no substantial correlation is found with alongshore wind stress. Cross-correlation analyses also reveal a lack of significant correlations across various time lags. On the other hand, (Bonino et al., 2019) found that local drivers and trends favoring upwelling (e.g., equatorward wind stress, cyclonic wind stress curl, and thermocline depth variation) explain the low-frequency modulation of upwelling. Bonino et al. (2019) also explored the link between wind-based upwelling indices and climate modes. They found that Atlantic and Pacific upwelling variabilities are mainly independent, while intra-basin domain variabilities present some coherency, which is consistent with our results. This intra-basin covariability is especially marked in the Pacific Ocean, where the shared variability is majorly due to the ENSO mode. In contrast, in the Atlantic Ocean, coherent variability is associated with upwelling trends, whereas only in the CanUS is it linked to the AMO. These results suggest that long-term climate indices may influence coastal upwelling dynamics, which is especially important in the Pacific. However, our index, $\alpha_{UI,}$ by normalizing the trend for its oceanic background, our results should account for the effects of local climate indices.

To assess Bakun's hypothesis and, thus, the upwelling capacity to overcome the oceanic warming effect, we define the angle ($\alpha_{UI,}$ readers are referred to section 3.3) between oceanic water and upwelling trends. Because this new index is directly based on trends, it captures only the low-frequency variability. Additionally, we verified the method's robustness using a probabilistic assessment of the uncertainties that showed consistent intensifications for all EBUS (Fig 5). This new approach differs from the traditional trend analysis since it normalizes the upwelling trends by comparing them with open ocean changes.

The EBUS in the Pacific Ocean yields minimum α_{UI} (10º±3º and 14º±3º for CalUS and HuUS, respectively), which is consistent with the low signal-to-noise ratio of global warming on this ocean, given its natural variability. The overall cooling signal caused by the IPO enhances the HuUS open ocean negative trends. Still, our index normalizes the upwelling trend to the full basin variability, suggesting the possibility of a mild Bakun effect even at the HuUS. In the Atlantic Ocean, the α_{UI} for the CanUS and BeUS are 20º±2º and 21º±2º, respectively, twice as large as in the Pacific Ocean. The α_{UI} presents wider angles at the southern hemisphere EBUS than in the northern hemisphere EBUS. Nevertheless, our results show a significant difference between oceanic and coastal trends reflected in positive α_{UI} in all EBUS (Fig 5).

The SST changes in the EBUS respond mainly to changes in the upwelling processes which are ultimately driven by the pressure gradients. We analyzed the pressure gradients trends in all four EBUS. Our findings further support the intensification of the pressure gradients driven by climate change, as stated by Bakun (1990). However, there are probably other contributors to the intensification of the upwellings. Some researchers question whether the impacts of differential heating on the pressure gradient force drives intensification of coastal upwelling. Rather, a complementary hypothesis proposes that evidence of an intensifying pressure gradient force is limited to poleward migration of the Hadley Cell (Arellano and Rivas, 2019; Rykaczewski et al., 2015; Wang et al., 2015). Nevertheless, these projections are only supported by observational records in the Humboldt and Benguela Systems, (Sydeman et al., 2014). In contrast, we have tested this hypothesis on the historical record by computing the latitudinal distribution of α_{UI}. The results shown in Fig 6 partially agree with Rykaczewski et al, (2015), as only CalUS and BeUS presented a poleward intensification of α_{UI}. To further understand the drivers of these changes, we examined the spatial stability of the trends in the SLP continental-oceanic gradient through Monte Carlo simulation. The discrepancy between the latitudinal distribution of α_{UI} and the small standard deviation of trends around the cores of the pressure systems suggests that the hypothesis of poleward displacement of the high-pressure systems remains inconclusive.

In summary, in this study, we use SST at discrete locations and the pressure gradient to explore the Bakun's hypothesis in the four major EBUS. Cooling trends are observed for all upwelling areas (the strongest in the HuUS and the weakest in the CalUS), and mainly warming trends offshore except for the HuUS. In addition, a novel index α_{UI} that normalizes the upwelling trends to their background open ocean trend is proposed. This index is easy to estimate, allows interbasin trend comparisons, and helps understand the role of changing upwellings in a changing climate. The index reveals that the Bakun hypothesis remains a possible mechanism for upwelling intensification in all four EBUS, although the Atlantic Basin shows a stronger intensification effect than the Pacific Ocean.

Data availability.

The moored data analyzed in this study are available at https://www.ndbc.noaa.gov/ and https://www.puertos.es/es-es/oceanografia/Paginas/portus.aspx for the Pacific and Atlantic Ocean, respectively. The cruise data are also available at https://calcofi.org/data/ for the Pacific Ocean and at https://www.seadatanet.org/ in the case of the Atlantic Ocean. For the Satellite-based data, the SST NOAA reanalysis product are avalaible from https://www.ncei.noaa.gov/data/sea-surface-temperature-optimum-interpolation/access/avhrr-only/. And the ERA5 data

Author contribution

M, Gutierrez-Guerra processed the data, and carried out all data analyses. M, Gutierrez-Guerra wrote the original paper with contributions from M, Gutierrez-Guerra, M.D, Perez-Hernandez and P, Velez. M.D, Perez-Hernandez and P, Velez supervised the study. All authors reviewed and edited the final paper.

Competing interests

The contact author has declared that none of the authors has any competing interest.

Acknowledgements

This article is a publication of the Unidad Océano y Clima from Universidad de Las Palmas de Gran Canaria, an R&D&I CSIC-associate unit. This work has been completed as part of the doctoral program in Oceanography and Global Change at the Instituto de Oceanografía y Cambio Global (IOCAG). M.A. Gutiérrez-Guerra acknowledges the Agencia Canaria de Investigación, Innovación y Sociedad de la Información (ACIISI) and the Fondo Social Europeo Plus (FSE+) Programa Operativo Integrado de

Canarias 2021-2027, Eje 3 Tema Prioritario 74 (85%) grant program of “Apoyo al personal investigador en formación” FPI2024010234 and the INVESTIGO grant program of “Plan de Recuperación, Transformación y Resiliencia – Next Generation EU”.

References

Abbott, M. R. and Zion, P. M.: Spatial and temporal variability of phytoplankton pigment off northern California during Coastal Ocean Dynamics Experiment 1, J Geophys Res Oceans, 92, 1745–1755, https://doi.org/10.1029/JC092IC02P01745, 1987.

Abrahams, A., Schlegel, R. W., and Smit, A. J.: Variation and Change of Upwelling Dynamics Detected in the World’s Eastern Boundary Upwelling Systems, Front Mar Sci, 8, 626411, https://doi.org/10.3389/FMARS.2021.626411/BIBTEX, 2021.

Andrews, W. R. H. and Cram, D. L.: Combined Aerial and Shipboard Upwelling Study in the Benguela Current, Nature 1969 224:5222, 224, 902–904, https://doi.org/10.1038/224902a0, 1969.

Andrews, W. R. H. and Hutchings, L.: Upwelling in the Southern Benguela Current, Prog Oceanogr, 9, 1–81, https://doi.org/10.1016/0079-6611(80)90015-4, 1980.

Arellano, B. and Rivas, D.: Coastal upwelling will intensify along the Baja California coast under climate change by mid-21st century: Insights from a GCM-nested physical-NPZD coupled numerical ocean model, Journal of Marine Systems, 199, 103207, https://doi.org/10.1016/J.JMARSYS.2019.103207, 2019.

Bakun, A.: Global climate change and intensification of coastal ocean upwelling, Science (1979), 247, 198–201, https://doi.org/10.1126/science.247.4939.198, 1990.

Bakun, A. and Nelson, C. S.: The Seasonal Cycle of Wind-Stress Curl in Subtropical Eastern Boundary Current Regions, J Phys Oceanogr, 21, 1815–1834, https://doi.org/https://doi.org/10.1175/1520-0485(1991)021<1815:TSCOWS>2.0.CO;2, 1991.

Bakun, A., Black, B. A., Bograd, S. J., García-Reyes, M., Miller, A. J., Rykaczewski, R. R., and Sydeman, W. J.: Anticipated Effects of Climate Change on Coastal Upwelling Ecosystems, Curr Clim Change Rep, 1, 85–93, https://doi.org/10.1007/s40641-015-0008-4, 2015.

Bang, N. and Andrews, W.: Direct current measurements of a shelf-edge frontal jet in the southern Benguela system, J Mar Res, 32, 1974.

Barton, E. D., Field, D. B., and Roy, C.: Canary current upwelling: More or less?, Prog Oceanogr, 116, 167–178, https://doi.org/10.1016/j.pocean.2013.07.007, 2013.

Belkin, I. M.: Rapid warming of Large Marine Ecosystems, Prog Oceanogr, 81, 207–213, https://doi.org/10.1016/j.pocean.2009.04.011, 2009.

Benazzouz, A., Mordane, S., Orbi, A., Chagdali, M., Hilmi, K., Atillah, A., Lluís Pelegrí, J., and Hervé, D.: An improved coastal upwelling index from sea surface temperature using satellite-based approach – The case of the Canary Current upwelling system, Cont Shelf Res, 81, 38–54, https://doi.org/10.1016/j.csr.2014.03.012, 2014.

Bonino, G., Di Lorenzo, E., Masina, S., and Iovino, D.: Interannual to decadal variability within and across the major Eastern Boundary Upwelling Systems, Scientific Reports 2019 9:1, 9, 1–14, https://doi.org/10.1038/s41598-019-56514-8, 2019.

Cropper, T. E., Hanna, E., and Bigg, G. R.: Spatial and temporal seasonal trends in coastal upwelling off Northwest Africa, 1981–2012, Deep Sea Research Part I: Oceanographic Research Papers, 86, 94–111, https://doi.org/10.1016/J.DSR.2014.01.007, 2014.

Demarcq, H.: Trends in primary production, sea surface temperature and wind in upwelling systems (1998-2007), Prog Oceanogr, 83, 376–385, https://doi.org/10.1016/j.pocean.2009.07.022, 2009.

Dugdale, R. C. and Wilkerson, F. P.: New production in the upwelling center at Point Conception, California: temporal and spatial patterns, Deep Sea Research Part A. Oceanographic Research Papers, 36, 985–1007, https://doi.org/10.1016/0198-0149(89)90074-5, 1989.

Ekman, V. W.: On the Influence of the Earth's Rotation on Ocean-Currents, Almqvist & Wiksells, Uppsala [Sweden], 1–52 pp., 1905.

Escribano, R., Daneri, G., Farías, L., Gallardo, V. A., González, H. E., Gutiérrez, D., Lange, C. B., Morales, C. E., Pizarro, O., Ulloa, O., and Braun, M.: Biological and chemical consequences of the 1997–1998 El Niño in the Chilean coastal upwelling system: a synthesis, Deep Sea Research Part II: Topical Studies in Oceanography, 51, 2389–2411, https://doi.org/10.1016/J.DSR2.2004.08.011, 2004.

Figueroa, D. and Moffat, C.: On the influence of topography in the induction of coastal upwelling along the Chilean Coast, Geophys Res Lett, 27, 3905–3908, https://doi.org/10.1029/1999GL011302, 2000.

García-Reyes, M., Sydeman, W. J., Schoeman, D. S., Rykaczewski, R. R., Black, B. A., Smit, A. J., and Bograd, S. J.: Under pressure: Climate change, upwelling, and eastern boundary upwelling ecosystems, Front Mar Sci, 2, 1–10, https://doi.org/10.3389/fmars.2015.00109, 2015.

Gómez-Gesteira, M., De Castro, M., Álvarez, I., Lorenzo, M. N., Gesteira, J. L. G., and Crespo, A. J. C.: Spatio-temporal upwelling trends along the Canary upwelling system (1967-2006), Ann N Y Acad Sci, 1146, 320–337, https://doi.org/10.1196/annals.1446.004, 2008.

Good, S. A., Corlett, G. K., Remedios, J. J., Noyes, E. J., and Llewellyn-Jones, D. T.: The global trend in sea surface temperature from 20 years of advanced very high resolution radiometer data, J Clim, 20, 1255–1264, https://doi.org/10.1175/JCLI4049.1, 2007.

Good, S. A., Martin, M. J., and Rayner, N. A.: EN4: Quality controlled ocean temperature and salinity profiles and monthly objective analyses with uncertainty estimates, J Geophys Res Oceans, 118, 6704–6716, https://doi.org/10.1002/2013JC009067, 2013.

Hutchings, L., van der Lingen, C. D., Shannon, L. J., Crawford, R. J. M., Verheye, H. M. S., Bartholomae, C. H., van der Plas, A. K., Louw, D., Kreiner, A., Ostrowski, M., Fidel, Q., Barlow, R. G., Lamont, T., Coetzee, J., Shillington, F., Veitch, J., Currie, J. C., and Monteiro, P. M. S.: The Benguela Current: An ecosystem of four components, Prog Oceanogr, 83, 15–32, https://doi.org/10.1016/j.pocean.2009.07.046, 2009.

Kämpf, J. and Chapman, P.: Upwelling Systems of the World, https://doi.org/10.1007/978-3-319-42524-5, 2016.

Kang, S. M., Yu, Y., Deser, C., Zhang, X., Kang, I. S., Lee, S. S., Rodgers, K. B., and Ceppi, P.: Global impacts of recent Southern Ocean cooling, Proc Natl Acad Sci U S A, 120, e2300881120, https://doi.org/10.1073/PNAS.2300881120/SUPPL_FILE/PNAS.2300881120.SAPP.PDF, 2023a.

Kang, S. M., Ceppi, P., Yu, Y., and Kang, I. S.: Recent global climate feedback controlled by Southern Ocean cooling, Nature Geoscience 2023 16:9, 16, 775–780, https://doi.org/10.1038/s41561-023-01256-6, 2023b.

Kendall, M.: Rank correlation methods (4th edn.) charles griffin, San Francisco, CA, 8, 875, 1975.

Lutjeharms, J. R. E. and Meeuwis, J. M.: The extent and variability of South-East Atlantic upwelling, South African Journal of Marine Science, 5, 51–62, https://doi.org/10.2989/025776187784522621, 1987.

Mann, H. B.: Nonparametric Tests Against Trend, Econometrica, 13, 245, https://doi.org/10.2307/1907187, 1945.

Marín, C.: Upwelling shadows at Mejillones Bay (northern Chilean coast): a remote sensing in situ analysis, Investigaciones Marinas, 31, 47–55, 2003.

McGregor, H. V., Dima, M., Fischer, H. W., and Mulitza, S.: Rapid 20th-century increase in coastal upwelling off northwest Africa, Science (1979), 315, 637–639, https://doi.org/10.1126/science.1134839, 2007.

Meehl, G. A., Hu, A., Santer, B. D., and Xie, S. P.: Contribution of the Interdecadal Pacific Oscillation to twentieth-century global surface temperature trends, Nature Climate Change 2016 6:11, 6, 1005–1008, https://doi.org/10.1038/nclimate3107, 2016.

Mesias, J. M., Matano, R. P., and Strub, P. T.: Dynamical analysis of the upwelling circulation off central Chile, J Geophys Res Oceans, 108, 3085, https://doi.org/10.1029/2001JC001135, 2003.

Narayan, N., Paul, A., Mulitza, S., and Schulz, M.: Trends in coastal upwelling intensity during the late 20th century, Ocean Science, 6, 815–823, https://doi.org/10.5194/OS-6-815-2010, 2010.

Pauly, D. and Christensen, V.: Primary production required to sustain global fisheries, Nature, 376, 279–279, https://doi.org/10.1038/376279b0, 1995.

Peard, K. R.: Seasonal and interannual variability of wind-driven upwelling at Lüderitz, Namibia, http://hdl.handle.net/11427/6498, 2007.

Reynolds, R. W., Smith, T. M., Liu, C., Chelton, D. B., Casey, K. S., and Schlax, M. G.: Daily high-resolution-blended analyses for sea surface temperature, J Clim, 20, 5473–5496, https://doi.org/10.1175/2007JCLI1824.1, 2007.

Rykaczewski, R. R., Dunne, J. P., Sydeman, W. J., García-Reyes, M., Black, B. A., and Bograd, S. J.: Poleward displacement of coastal upwelling-favorable winds in the ocean's eastern boundary currents through the 21st century, Geophys Res Lett, 42, 6424–6431, https://doi.org/10.1002/2015GL064694, 2015.

Sambe, B., Tandstad, M., Caramelo, A. M., and Brownd, B. E.: Variations in productivity of the Canary Current Large Marine Ecosystem and their effects on small pelagic fish stocks, Environ Dev, 17, 105–117, https://doi.org/10.1016/j.envdev.2015.11.012, 2016.

Santos, F., deCastro, M., Gómez-Gesteira, M., and Álvarez, I.: Differences in coastal and oceanic SST warming rates along the Canary upwelling ecosystem from 1982 to 2010, Cont Shelf Res, 47, 1–6, https://doi.org/10.1016/j.csr.2012.07.023, 2012.

Seabra, R., Varela, R., Santos, A. M., Gómez-Gesteira, M., Meneghesso, C., Wethey, D. S., and Lima, F. P.: Reduced nearshore warming associated with eastern boundary upwelling systems, Front Mar Sci, 6, 445128, https://doi.org/10.3389/FMARS.2019.00104/BIBTEX, 2019.

Sherman, K. and Hempel, G.: The UNEP Large Marine Ecosystem Report: A perspective on changing conditions in LMEs of the world's Regional Seas, UNEP Regional Seas Reports and Studies , 2008.

Siemer, J. P., Machín, F., González-Vega, A., Arrieta, J. M., Gutiérrez-Guerra, M. A., Pérez-Hernández, M. D., Vélez-Belchí, P., Hernández-Guerra, A., and Fraile-Nuez, E.: Recent Trends in SST, Chl-a, Productivity and Wind Stress in Upwelling and Open Ocean Areas in the Upper Eastern North Atlantic Subtropical Gyre, J Geophys Res Oceans, 126, e2021JC017268, https://doi.org/10.1029/2021JC017268, 2021.

Signorini, S. R., Franz, B. A., and McClain, C. R.: Chlorophyll variability in the oligotrophic gyres: Mechanisms, seasonality and trends, Front Mar Sci, 2, 1–11, https://doi.org/10.3389/fmars.2015.00001, 2015.

Smale, D. A. and Wernberg, T.: Satellite-derived SST data as a proxy for water temperature in nearshore benthic ecology, Mar Ecol Prog Ser, 387, 27–37, https://doi.org/10.3354/MEPS08132, 2009.

Sydeman, W. J., García-Reyes, M., Schoeman, D. S., Rykaczewski, R. R., Thompson, S. A., Black, B. A., and Bograd, S. J.: Climate change and wind intensification in coastal upwelling ecosystems, Science (1979), 345, 77–80, https://doi.org/10.1126/science.1251635, 2014.

Tel, E., Balbin, R., Cabanas, J. M., Garcia, M. J., Carmen Garcia-Martinez, M., Gonzalez-Pola, C., Lavin, A., Lopez-Jurado, J. L., Rodriguez, C., Ruiz-Villarreal, M., Sánchez-Leal, R. F., Vargas-Yáñez, M., and Vélez-Belchí, P.: IEOOS: The Spanish Institute of Oceanography Observing System, Ocean Science, 12, 345–353, https://doi.org/10.5194/OS-12-345-2016, 2016.

Wang, D., Gouhier, T. C., Menge, B. A., and Ganguly, A. R.: Intensification and spatial homogenization of coastal upwelling under climate change, Nature, 518, 390–394, https://doi.org/10.1038/nature14235, 2015.